Monthly Notices
of the
ROYAL ASTRONOMICAL SOCIETY

MNRAS **502,** L79–L84 (2021)
Advance Access publication 2021 January 06

doi:10.1093/mnrasl/slab006

ALMA detection of millimetre 183 GHz H_2O maser emission in the Superantennae galaxy at $z \sim 0.06$

Masatoshi Imanishi,[1,2]★ Yoshiaki Hagiwara,[3] Shinji Horiuchi,[4] Takuma Izumi [1,2] and Kouichiro Nakanishi [1,2]

[1]*National Astronomical Observatory of Japan, National Institutes of Natural Sciences (NINS), 2-21-1 Osawa, Mitaka, Tokyo 181-8588, Japan*
[2]*Department of Astronomy, School of Science, The Graduate University for Advanced Studies, SOKENDAI, Mitaka, Tokyo 181-8588, Japan*
[3]*Natural Science Laboratory, Toyo University, 5-28-20 Hakusan, Bunkyo-ku, Tokyo 112-8606, Japan*
[4]*CSIRO Astronomy and Space Science, Canberra Deep Space Communications Complex, PO Box 1035, Tuggeranong, ACT 2901, Australia*

Accepted 2021 January 11. Received 2021 January 8; in original form 2020 December 14

ABSTRACT

We present the results of Atacama Large Millimeter/submillimeter Array (ALMA) band-5 (∼170 GHz) observations of the merging ultraluminous infrared galaxy, the 'Superantennae' (IRAS 19254−7245), at $z = 0.0617$, which has been diagnosed as containing a luminous obscured active galactic nucleus (AGN). In addition to dense molecular line emission (HCN $J = 2$–1, HCO^+ $J = 2$–1, and HNC $J = 2$–1), we detect a highly luminous ($\sim 6 \times 10^4\,L_\odot$) 183 GHz H_2O $3_{1,3}$–$2_{2,0}$ emission line. We interpret the strong H_2O emission as largely originating in maser amplification in AGN-illuminated dense and warm molecular gas, based on (1) the spatially compact ($\lesssim$220 pc) nature of the H_2O emission, unlike spatially resolved ($\gtrsim$500 pc) dense molecular emission, and (2) a strikingly different velocity profile from, and (3) significantly elevated flux ratio relative to, dense molecular emission lines. H_2O maser emission, other than the widely studied 22 GHz $6_{1,6}$–$5_{2,3}$ line, has been expected to provide important information on the physical properties of gas in the vicinity of a central mass-accreting supermassive black hole (SMBH), because of different excitation energy. We here demonstrate that with highly sensitive ALMA, millimetre 183 GHz H_2O maser detection is feasible out to >270 Mpc, opening a new window to scrutinize molecular gas properties around a mass-accreting SMBH far beyond the immediately local Universe.

Key words: masers – galaxies: active – galaxies: individual: IRAS 19254−7245 (Superantennae) – galaxies: nuclei – quasars: supermassive black holes – radio lines: galaxies.

1 INTRODUCTION

Water (H_2O) is an abundant molecule in the Universe and has been detected in many active galaxies (Yang, Gao & Omont 2013). The rotational energy levels of H_2O are more complex than those of simple molecules (e.g. CO, HCN) and many rotational transition lines are found in the far-infrared (70–300 μm), (sub)millimetre (0.3–10 mm), and centimetre (>1 cm) wavelength ranges. In dense and warm molecular gas, population inversion can occur for a number of H_2O rotational transitions through collisional excitation and/or infrared radiative pumping (e.g. Yates, Field & Gray 1997; Gonzalez-Alfonso et al. 2010). This population inversion can amplify background radiation and these H_2O emission lines can be extremely bright through maser phenomena. The luminous megamaser ($> 10\,L_\odot$) emission line of *ortho*-H_2O $6_{1,6}$–$5_{2,3}$ at rest frequency $\nu_{\rm rest} \sim 22$ GHz (1.35 cm) has been detected in galaxy nuclei, mostly obscured active galactic nuclei (AGNs; e.g. Braatz, Wilson & Henkel 1996; Greenhill et al. 2003a; Braatz et al. 2004; Henkel et al. 2005; Kondratko, Greenhill & Moran 2006a; Kondratko et al. 2006b), out to $z \sim 0.66$ for an unlensed AGN (Barvainis & Antonucci 2005) and $z \sim 2.6$ for a lensed AGN (Impellizzeri et al. 2008). Dense and warm molecular gas in the vicinity of a luminous AGN is a plausible site for this H_2O megamaser emission (Neufeld, Maloney & Conger 1994; Maloney et al. 2002), which often shows brighter blueshifted and redshifted components than the systemic velocity component caused by a highly edge-on rotating disc. Because high-spatial-resolution very-long-baseline interferometry (VLBI) observations are possible at centimetre wavelengths, detailed spatially resolved dynamical studies of the bright 22 GHz H_2O megamaser emission can be an excellent probe of the surrounding mass distribution. Such VLBI observations provided the first convincing evidence of the presence of a supermassive black hole (SMBH) and its precise mass measurement in the nearby AGN NGC 4258 at ∼7 Mpc (Miyoshi et al. 1995). Subsequent centimetre VLBI observations also revealed the dynamical properties of H_2O megamaser-emitting gas in close proximity to central mass-accreting SMBHs and constrained SMBH masses in other nearby well-studied AGNs, including NGC 4945 at ∼4 Mpc (Greenhill, Moran & Herrnstein 1997), Circinus at ∼4 Mpc (Greenhill et al. 2003b), and others (e.g. Kuo et al. 2011).

Theoretically, other H_2O rotational transition lines in the (sub)millimetre wavelength range can also be extremely bright as a result of the maser phenomena caused by population inversion in dense and warm molecular gas. Examples include the $3_{1,3}$–$2_{2,0}$ transition line of *para*-H_2O at $\nu_{\rm rest} \sim 183$ GHz, $10_{2,9}$–$9_{3,6}$ line of *ortho*-H_2O at $\nu_{\rm rest} \sim 321$ GHz, and $5_{1,5}$–$4_{2,2}$ line of *para*-H_2O at $\nu_{\rm rest}$

★ E-mail: masa.imanishi@nao.ac.jp

$\sim$ 325 GHz (e.g. Deguchi 1977; Neufeld & Melnick 1991; Yates et al. 1997). Observing multiple H_2O megamaser emission lines will enable us to constrain the physical properties of the innermost AGN-illuminated gas around a mass-accreting SMBH (Maloney et al. 2002; Hagiwara et al. 2013), because excitation energy levels differ distinctly between different lines.

With the advent of highly sensitive (sub)millimetre observing facilities, including the Atacama Large Millimeter/submillimeter Array (ALMA), detection of (sub)millimetre H_2O emission (183 GHz H_2O $3_{1,3}$–$2_{2,0}$ and/or 321 GHz H_2O $10_{2,9}$–$9_{3,6}$ lines) has been reported in the very nearby obscured AGNs: Circinus ($\sim$4 Mpc), NGC 4945 ($\sim$4 Mpc), and NGC 3079 ($\sim$16 Mpc; Humphreys et al. 2005, 2016; Hagiwara et al. 2013, 2016; Pesce, Braatz & Impellizzeri 2016). These detected (sub)millimetre H_2O emission lines can be explained by maser phenomena based mainly on high luminosity and velocity profiles similar to the 22 GHz H_2O megamaser emission previously detected by VLBI observations. The 183 GHz H_2O emission line was also detected in the infrared luminous merging galaxy Arp 220 at $z \sim 0.018$ ($\sim$80 Mpc; Cernicharo, Pardo & Weiss 2006). While Cernicharo et al. (2006) interpreted the emission as masers originating from nuclear star-forming regions, Hagiwara et al. (2016) and Galametz et al. (2016) argued that it is more likely to be thermal emission. Konig et al. (2017) later detected the 183 and 325 GHz H_2O emission lines in Arp 220 and preferred the hypothesis of masers from star-forming regions (not from an AGN). Despite the potential importance of (sub)millimetre H_2O megamaser emission from AGN-illuminated molecular gas, it remains largely unexplored beyond the immediately local Universe at >20 Mpc.

In this paper, we report the detection of notably luminous 183 GHz H_2O emission that is interpreted as being of maser origin, in the obscured-AGN-hosting infrared luminous merging galaxy, the 'Superantennae', at $z = 0.0617$. Adopting $H_0 = 71$ km s^{-1} Mpc^{-1}, $\Omega_m = 0.27$, and $\Omega_\Lambda = 0.73$, its luminosity distance is 273 Mpc and 1 arcsec corresponds to 1.2 kpc.

2 TARGET

The 'Superantennae' (IRAS 19254−7245) is a merging galaxy in the Southern hemisphere (declination $\sim -72^\circ$), consisting of two galaxy nuclei with a separation of $\sim$8 arcsec ($\sim$10 kpc) along the north–south direction and prominent long (>300 kpc) tidal tails (Melnick & Mirabel 1990; Mirabel, Lutz & Maza 1991; Duc, Mirabel & Maza 1997). It has infrared luminosity $L_{IR} \sim 1 \times 10^{12}$ L$_\odot$ (Melnick & Mirabel 1990), belonging to the class of ultraluminous infrared galaxies (ULIRGs; Sanders & Mirabel 1996). The Superantennae is a scaled-up version of the classical merging galaxy 'Antennae' (NGC 4038/9), with >3 times longer tidal tails and $\sim$10 times higher infrared luminosity (Sanders & Mirabel 1996). The southern nucleus is classified as an obscured AGN through optical spectroscopy (Colina, Lipari & Macchetto 1991; Mirabel et al. 1991; Duc et al. 1997; Kewley et al. 2001), and signatures of a luminous obscured AGN behind a large column density of material were also found based on >2 μm infrared spectroscopy (Genzel et al. 1998; Vanzi et al. 2002; Risaliti et al. 2003; Reunanen, Tacconi-Garman & Ivanov 2007; Imanishi et al. 2008; Nardini et al. 2009, 2010) and >2 keV X-ray spectroscopy (Imanishi & Ueno 1999; Pappa, Georgantopoulos & Stewart 2000; Braito et al. 2003, 2009; Jia et al. 2012).

3 OBSERVATIONS AND DATA ANALYSIS

The 183 GHz H_2O line data of the Superantennae were obtained in our ALMA Cycle 5 program 2017.1.00022.S (PI: M. Imanishi) as part of band-5 (163–211 GHz) observations of $z < 0.15$ ULIRGs with dense molecular tracers HCN $J = 2$–1 ($\nu_{rest} = 177.261$ GHz), HCO$^+$ $J = 2$–1 ($\nu_{rest} = 178.375$ GHz), and HNC $J = 2$–1 ($\nu_{rest} = 181.325$ GHz; Imanishi et al., in preparation). The H_2O $3_{1,3}$–$2_{2,0}$ line ($\nu_{rest} = 183.310$ GHz) data were simultaneously obtained with the HNC $J = 2$–1 line data on 2018 September 18 (UT) with 43 antennas with 15–1398 m baselines. The bandpass, flux, and phase calibrator were J1617−5848, J1617−5848, and J1837−7108, respectively. The net on-source integration time was 27 min. HCN $J = 2$–1 and HCO$^+$ $J = 2$–1 line data were taken separately on 2018 September 18 (UT) with the same antenna numbers, baselines, and calibrators. The net on-source integration time was 6 min.

We used CASA (https://casa.nrao.edu) for the reduction of data calibrated and provided by ALMA. We selected channels that displayed no obvious emission lines to determine the continuum level, and then subtracted it using the CASA task 'uvcontsub'. The 'clean' task was applied with Briggs weighting (robust = 0.5 and gain = 0.1) for both the continuum-only and continuum-subtracted molecular line data, with a pixel scale of 0.05 arcsec pixel^{-1}. The synthesized beam size was $\sim$0.55 arcsec × 0.35 arcsec ($\sim$650 pc × 400 pc).

4 RESULTS

Continuum emission is clearly detected at International Celestial Reference System (ICRS) coordinates of ($19^h31^m21\overset{s}{.}43$, $-72^\circ39'21\overset{''}{.}5$) (i.e. southern nucleus) and is displayed as contours in Fig. 1 (top). In Fig. 1 (top), integrated intensity (moment 0) maps of the 183 GHz H_2O, HNC $J = 2$–1, HCO$^+$ $J = 2$–1, and HCN $J = 2$–1 lines are shown as images. These molecular emission line peak positions spatially agree with the continuum peak. Table 1 (columns 1–4) summarizes these molecular emission line properties.

Figs 2(a)–(b) show beam-sized spectra at the continuum peak, where the 183 GHz H_2O $3_{1,3}$–$2_{2,0}$ line and HNC $J = 2$–1, HCO$^+$ $J = 2$–1, and HCN $J = 2$–1 emission lines are clearly detected. The 183 GHz H_2O emission line is characterized by a double-peaked profile, whereas the remaining three dense molecular tracers (HNC $J = 2$–1, HCO$^+$ $J = 2$–1, and HCN $J = 2$–1) display single-peaked emission line profiles. We apply a double and single Gaussian fit for the 183 GHz H_2O and dense molecular lines, respectively. Table 1 (columns 5–8) summarizes the fitting results.

Intensity-weighted mean velocity (moment 1) and intensity-weighted velocity dispersion (moment 2) maps of 183 GHz H_2O, HNC $J = 2$–1, HCO$^+$ $J = 2$–1, and HCN $J = 2$–1 lines are displayed in Figs 1(e)–(l). A similar rotation pattern is seen for the HNC $J = 2$–1, HCO$^+$ $J = 2$–1, and HCN $J = 2$–1 lines, with the south-eastern side being blueshifted and the north-western side being redshifted (Figs 1f–h), as previously seen for other dense molecular tracers, HCN $J = 3$–2 and HCO$^+$ $J = 3$–2 (Imanishi, Nakanishi & Izumi 2016), and near-infrared ($\sim$2 μm) emission lines (Reunanen et al. 2007). However, the 183 GHz H_2O emission line shows no such rotation signature (Fig. 1e), and yet shows much larger velocity dispersion values of >200 km s^{-1} than the three dense molecular tracers at the nuclear ($\lesssim$1 kpc) region (Figs 1i–l). It is suggested that H_2O and dense molecular emission originate from dynamically and spatially different regions in the galaxy nucleus.

5 DISCUSSION

In the Superantennae, the 183 GHz H_2O-to-HNC $J = 2$–1 flux ratio is $\sim$4 (Table 1), which is by far the largest among $z < 0.15$ ULIRGs, the ratios of which are $\lesssim$2 (Imanishi et al., in preparation). The Superantennae is an outlier in this flux ratio. HNC emission is

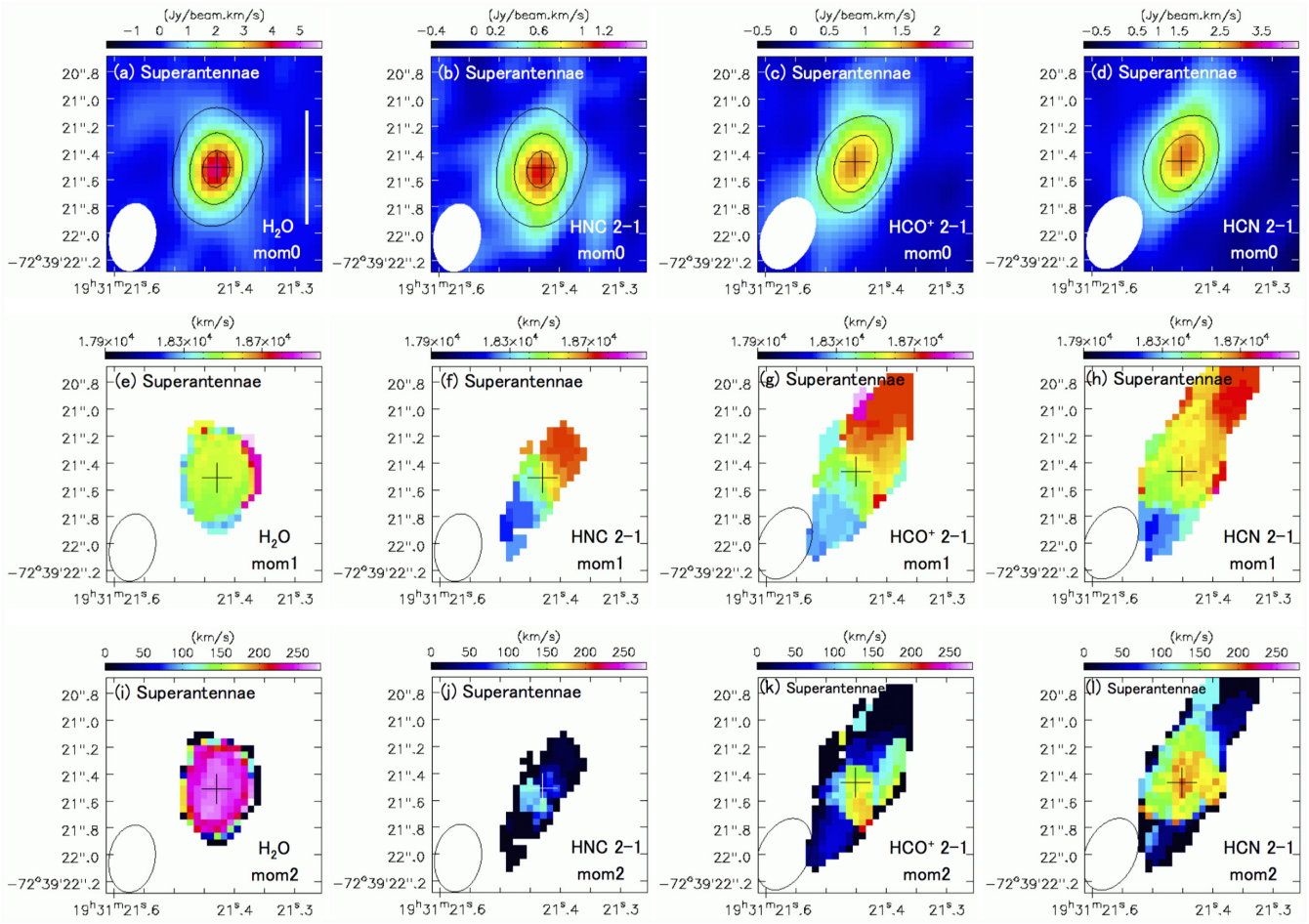

Figure 1. (*Top*) Integrated intensity (moment 0) map of (a) 183 GHz H_2O $3_{1,3}$–$2_{2,0}$, (b) HNC $J = 2$–1, (c) HCO^+ $J = 2$–1, and (d) HCN $J = 2$–1 lines in ICRS coordinates. Continuum emission simultaneously taken with individual lines is shown as contours [5σ, 15σ, and 25σ with rms = 0.11 (mJy beam^{-1}) for the left two panels and 5σ and 10σ with rms = 0.21 (mJy beam^{-1}) for the right two panels]. The continuum peak flux is 3.4 (mJy beam^{-1}; 30σ) and 3.1 (mJy beam^{-1}; 15σ) for the left and right pair of panels, respectively. The vertical white bar in (a) corresponds to 1 kpc. (*Middle*) Intensity-weighted mean velocity (moment 1) map of the same lines. (*Bottom*) Intensity-weighted velocity dispersion (moment 2) map. In (a)–(l), the continuum peak position is shown as a cross. The filled or open circle in the lower left part indicates the synthesized beam size of each moment map. An appropriate cut-off ($\sim 2\sigma$) is applied to the moment 1 and 2 maps to prevent them from being dominated by noise.

Table 1. Molecular emission-line properties.

Line	Integrated intensity (moment 0) map			Gaussian fit			
	Peak (Jy beam^{-1})	rms (km s^{-1})	Beam (arcsec × arcsec) (°)	Velocity (km s^{-1})	Peak (mJy)	FWHM (km s^{-1})	Flux (Jy km s^{-1})
(1)	(2)	(3)	(4)	(5)	(6)	(7)	(8)
183 GHz H_2O	4.3 (15σ)	0.30	0.50 × 0.34 (−10)	18205 ± 14, 18738 ± 20[a]	5.2 ± 0.3, 4.9 ± 0.2[a]	357 ± 30, 562 ± 46[a]	4.6 ± 0.3
HNC J = 2–1	1.1 (5.0σ)	0.23	0.51 × 0.35 (−9)	18547 ± 31	1.8 ± 0.2	649 ± 98	1.2 ± 0.2
HCO^+ J = 2–1	1.6 (6.3σ)	0.29	0.56 × 0.37 (−26)	18522 ± 24	2.6 ± 0.2	767 ± 61	2.0 ± 0.2
HCN J = 2–1	2.9 (6.3σ)	0.47	0.57 × 0.37 (−26)	18564 ± 17	3.8 ± 0.2	810 ± 48	3.1 ± 0.2

Notes. Col. (1): Line. Col. (2): Integrated intensity (in Jy beam^{-1} km s^{-1}) at the emission peak. Detection significance relative to the rms noise (1σ) in the moment 0 map is shown in parentheses. Col. (3): Rms noise (1σ) level in the moment 0 map (in Jy beam^{-1} km s^{-1}), derived from the standard deviation of sky signals in each moment 0 map. Col. (4): Beam size (in arcsec × arcsec) and position angle (in degrees). The position angle is 0° along the north–south direction, and increases counterclockwise. Cols. (5)–(8): Gaussian fit of emission line in the spectrum at the continuum peak position, within the beam size. Col. (5): Optical local standard of rest (LSR) velocity (v_{opt}) of the emission line peak (in km s^{-1}). Col. (6): Peak flux (in mJy). Col. (7): Observed full width at half-maximum (FWHM) (in km s^{-1}). Col. (8): Gaussian-fit, velocity-integrated flux (in Jy km s^{-1}). This flux will be used for our discussion of flux ratios.
[a]Two Gaussian fit.

sometimes observed to be weak in the vicinity of a luminous AGN if the column density of the surrounding molecular gas is insufficient for HNC shielding (e.g. Imanishi, Nakanishi & Izumi 2018; Imanishi et al. 2020). In fact, in the Superantennae, the flux of HNC, relative to HCN, at $J = 3$–2 and $J = 4$–3 is smaller than those of other ULIRGs (Imanishi et al. 2018). To distinguish whether (1) the 183 GHz H_2O

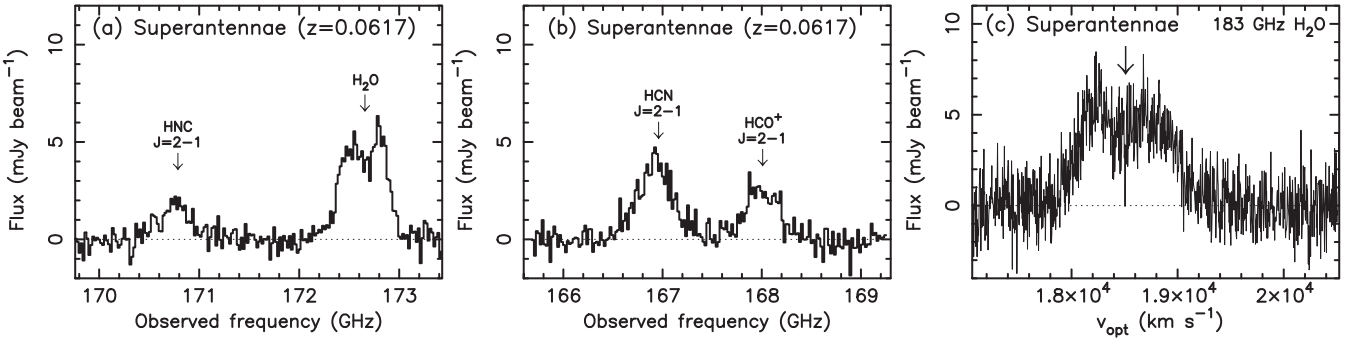

Figure 2. Spectrum of (a) 183 GHz H_2O $3_{1,3}$–$2_{2,0}$ and HNC $J = 2$–1 and (b) HCN $J = 2$–1 and HCO^+ $J = 2$–1 lines. The abscissa is observed frequency (in GHz) and the ordinate is flux density (in mJy beam^{-1}). The rms noise level is ∼1 mJy beam^{-1} for ∼35 km s^{-1} resolution. (c) Detailed velocity profile of the 183 GHz H_2O $3_{1,3}$–$2_{2,0}$ emission line. The abscissa is optical LSR velocity (in km s^{-1}) with ∼3.5 km s^{-1} resolution and the ordinate is flux density (in mJy beam^{-1}). The downward arrow indicates the systemic velocity (18510 km s^{-1}) of the Superantennae.

emission line is strong or (2) the HNC $J = 2$–1 emission line is weak, we investigate the 183 GHz H_2O-to-HCO^+ $J = 2$–1 flux ratio of the Superantennae and find it to be >2 (Table 1), which is also significantly higher than the ratios of $\lesssim$1 in the majority of other ULIRGs (Imanishi et al., in preparation). The H_2O-to-HCN $J = 2$–1 flux ratio of the Superantennae (>1.4; Table 1) is also significantly higher than those of other ULIRGs ($\lesssim$1; Imanishi et al., in preparation). As HCN $J = 2$–1 emission can be enhanced in AGNs (e.g. Kohno 2005; Imanishi et al. 2007, 2009, 2016; Krips et al. 2008; Izumi et al. 2016; Imanishi, Nakanishi & Izumi 2019), we thought that the excess H_2O-to-HCN $J = 2$–1 flux ratio in the Superantennae may be weaker than other flux ratios, and yet it is still higher than those of other ULIRGs. To summarize, in the Superantennae, the 183 GHz H_2O emission is significantly elevated relative to dense molecular line emission HNC $J = 2$–1, HCO^+ $J = 2$–1, and HCN $J = 2$–1. Applying equation (3) of Solomon & Vanden Bout (2005) to the observed emission line flux in Table 1 (column 8), the luminosity in units of (K km s^{-1} pc^2) is estimated to be 0.83×10^8, 1.4×10^8, and 2.3×10^9 for HNC $J = 2$–1, HCO^+ $J = 2$–1, and HCN $J = 2$–1, respectively. The probed nuclear dense molecular mass in the beam-sized spectrum (0.55 arcsec × 0.35 arcsec or 650 pc × 400 pc) is higher than a few $\times 10^8 M_\odot$, where we (1) use HCO^+ $J = 2$–1 luminosity as the least biased dense molecular mass indicator (see the above-mentioned possible ambiguity for HNC and HCN around a luminous AGN), (2) assume that HCO^+ emission is optically thick and thermalized at $J = 2$–1 and $J = 1$–0 (i.e. same luminosity between $J = 2$–1 and $J = 1$–0 in units of K km s^{-1} pc^2), and (3) adopt a luminosity-to-mass conversion factor of 2–5 [$M_\odot$ (K km s^{-1} pc^2)$^{-1}$] for HCO^+ $J = 1$–0 (Leroy et al. 2017). The strong 183 GHz H_2O emission, even compared with the emission from such high-mass nuclear dense molecular gas, is remarkable.

We interpret that maser amplification of the 183 GHz H_2O emission line is a plausible physical mechanism for its flux elevation. First, while similar rotation patterns are seen in the moment 1 maps of the HNC $J = 2$–1, HCO^+ $J = 2$–1, and HCN $J = 2$–1 lines (Figs 1f–h), and so these emissions are spatially resolved, the lack of such rotation patterns (Fig. 1e) suggests that the 183 GHz H_2O emission originates in very compact, spatially unresolved molecular gas. We apply the CASA task 'imfit' to moment 0 maps (Figs 1a–d) and find that the deconvolved intrinsic emission size of H_2O ($\lesssim$180 mas or $\lesssim$220 pc) is much smaller than those of HCN $J = 2$–1, HCO^+ $J = 2$–1, and HNC $J = 2$–1 (450–1050 mas or 550–1250 pc). This is also confirmed by visibility fitting, using the CASA task 'uvmodelfit'. AGN-illuminated dense and warm molecular gas with coherent velocity at the very centre (<<1 kpc) of the nucleus is the most plausible site for maser amplification (Neufeld et al. 1994; Maloney et al. 2002) and can naturally explain the compact, spatially unresolved 183 GHz H_2O emission.

Second, unlike dense molecular tracers with single-peaked emission line profiles, the 183 GHz H_2O emission line is double peaked. This double-peaked emission line profile, by definition, can produce large velocity dispersion values in the moment 2 map of the H_2O line (Fig. 1i). Fig. 2(c) shows the detailed profile of the H_2O emission line with finer velocity resolution (∼3.5 km s^{-1}), where the blueshifted and redshifted emission components are brighter than the systemic velocity component, as often seen in the bright 22 GHz H_2O megamaser emission in AGNs (e.g. Braatz et al. 1996, 2004; Greenhill et al. 2003a; Henkel et al. 2005; Kondratko et al. 2006a, b). The observed double-peaked emission line profile of the Superantennae can naturally be reproduced if maser-origin blueshifted and redshifted H_2O emission in the vicinity of the mass-accreting SMBH is superposed on to very broad (FWHM ∼ 650–800 km s^{-1}; Table 1) thermal H_2O emission from the galaxy nucleus (∼1 kpc). A compact rotating maser disc at both sides of the central mass-accreting SMBH can produce stronger blueshifted and redshifted emission than the systemic velocity component at the foreground side of the SMBH (Miyoshi et al. 1995). The 183 GHz H_2O emission detected in other $z < 0.15$ ULIRGs shows a single-peaked line profile, similar to those of dense molecular tracers (Imanishi et al., in preparation). To summarize, the luminous, spatially compact, spectrally double-peaked 183 GHz H_2O emission in the Superantennae can naturally be explained by maser amplification in AGN-illuminated gas at the very centre of the galaxy nucleus, and an enhanced H_2O abundance in a large volume of nuclear (∼1 kpc) dense molecular gas is disfavoured as the origin of the elevated 183 GHz H_2O emission. While a large fraction of AGNs with detected 22 GHz H_2O megamaser emission show multiple narrow features, the maser-origin 183 GHz H_2O emission of the Superantennae is broad, as seen in a few AGNs for the 22 GHz line (e.g. Koekemoer et al. 1995; Braatz et al. 1996). We interpret that H_2O maser spots in the Superantennae distribute widely and continuously along the radial direction from the central mass-accreting SMBH.

The observed 183 GHz H_2O emission line properties in the Superantennae are significantly different from those of another ULIRG with 183 GHz H_2O emission line detection, Arp 220 (z = 0.018 or ∼80 Mpc; Cernicharo et al. 2006; Galametz et al. 2016; Konig et al. 2017). In Arp 220, the 183 GHz H_2O emission line flux is smaller than those of the HNC $J = 2$–1, HCO^+ $J = 2$–1, and

HCN $J = 2$–1 lines (Galametz et al. 2016), similar to the majority of $z < 0.15$ ULIRGs (Imanishi et al., in preparation). The line profile of the 183 GHz H_2O emission in Arp 220 is also single peaked in a similar way to those of dense molecular lines (Cernicharo et al. 2006; Galametz et al. 2016; Konig et al. 2017). These observational results of the 183 GHz H_2O emission in Arp 220 can naturally be explained by thermal emission. The Superantennae shows the strongest AGN-origin megamaser emission signatures for the 183 GHz H_2O line beyond the immediately local Universe at >20 Mpc.

Adopting equation (1) of Solomon & Vanden Bout (2005), we obtain the 183 GHz H_2O maser (isotropic) luminosity $L_{183\mathrm{GHz}-H_2O} \sim 6.1 \times 10^4\,L_\odot$. Even though a fraction of this H_2O luminosity comes from thermal emission in the nuclear region (∼1 kpc) of the galaxy, the fact that the H_2O-to-HCO^+ $J = 2$–1 and H_2O-to-HNC $J = 2$–1 flux ratios in the Superantennae are $\gtrsim$2 times higher than those in other $z < 0.15$ ULIRGs suggests that at least half the luminosity (higher than a few $\times 10^4\,L_\odot$) originates from maser emission from the AGN-illuminated gas (<<1kpc). This is as high as or possibly even higher than the most luminous 22 GHz H_2O megamaser emission in an AGN at $z \sim 0.66$ ($\sim 2 \times 10^4\,L_\odot$; Barvainis & Antonucci 2005). The Superantennae is a promising target for detecting multiple H_2O megamaser emission lines to constrain the physical properties of AGN-illuminated dense and warm molecular gas around an actively mass-accreting SMBH. The upper and lower energy levels of H_2O lines are (E_u, E_l) = (643 K, 642 K) for the $6_{1,6}$–$5_{2,3}$ transition at 22 GHz, and (205 K, 196 K) for the $3_{1,3}$–$2_{2,0}$ transition at 183 GHz. Depending on molecular gas temperature, the 183 Ghz to 22 GHz H_2O maser flux ratio can vary widely (Cernicharo et al. 2006). For the Superantennae, no detection was reported for the well-studied 22 GHz H_2O maser emission with shallow (rms $\gtrsim$ 75 mJy) observations (Greenhill et al. 2002). More sensitive 22 GHz observations will provide important insights into the properties of AGN-illuminated gas at the very centre of galaxy nuclei in the distant Universe at >270 Mpc.

6 SUMMARY

We conducted ALMA band-5 observations of the Superantennae galaxy at $z = 0.0617$. We detected remarkably strong 183 GHz H_2O $3_{1,3}$–$2_{2,0}$ emission, relative to dense molecular lines (HNC $J = 2$–1, HCO^+ $J = 2$–1, and HCN $J = 2$–1) when compared to other ULIRGs. The observed compact, spatially unresolved emission nature and double-peaked emission line profile of H_2O are markedly different from the spatially resolved, single-peaked emission line properties of dense molecular tracers in the galaxy nucleus. We argue that the detected luminous 183 GHz H_2O emission originates in maser amplification in AGN-illuminated molecular gas around a mass-accreting SMBH at the very centre of the galaxy nucleus. This pushes (sub)millimetre H_2O maser emission detection up to >270 Mpc, far beyond the immediately local Universe, owing to ALMA's high sensitivity. Combination with so-far undetected 22 GHz H_2O maser emission will constrain the physical properties of dense and warm molecular gas in the vicinity of a mass-accreting SMBH.

ACKNOWLEDGEMENTS

We thank the referee for valuable comments. This paper makes use of the following ALMA data: ADS/JAO.ALMA#2017.1.00022.S. Data analysis was in part carried out on the open use data analysis computer system at the Astronomy Data Center of the National Astronomical Observatory of Japan.

DATA AVAILABILITY

The data used in this paper (2017.1.00022.S) are available in the ALMA archive at https://almascience.eso.org/.

REFERENCES

Barvainis R., Antonucci R., 2005, ApJ, 628, L89
Braatz J. A., Wilson A. S., Henkel C., 1996, ApJS, 106, 51
Braatz J. A., Henkel C., Greenhill L. J., Moran J. M., Wilson A. S., 2004, ApJ, 617, L29
Braito V. et al., 2003, A&A, 398, 107
Braito V., Reeves J. N., Della Ceca R., Ptak A., Risaliti G., Yaqoob T., 2009, A&A, 504, 53
Cernicharo J., Pardo J. R., Weiss A., 2006, ApJ, 646, L49
Colina L., Lipari S., Macchetto F., 1991, ApJ, 379, 113
Deguchi S., 1977, PASJ, 29, 669
Duc P.-A., Mirabel I. F., Maza J., 1997, A&AS, 124, 533
Galametz M. et al., 2016, MNRAS, 462, L36
Genzel R. et al., 1998, ApJ, 498, 579
Gonzalez-Alfonso E. et al., 2010, A&A, 518, L43
Greenhill L. J., Moran J. M., Herrnstein J. R., 1997, ApJ, 481, L23
Greenhill L. J. et al., 2002, ApJ, 565, 836
Greenhill L. J., Kondratko P. T., Lovell J. E. J., Kuiper T. B. H., Moran J. M., Jauncey D. L., Baines G. P., 2003a, ApJ, 582, L11
Greenhill L. J. et al., 2003b, ApJ, 590, 162
Hagiwara Y., Miyoshi M., Doi A., Horiuchi S., 2013, ApJ, 768, L38
Hagiwara Y., Horiuchi S., Doi A., Miyoshi M., Edwards P. G., 2016, ApJ, 827, 69
Henkel C., Peck A. B., Tarchi A., Nagar N. M., Braatz J. A., Castangia P., Moscadelli L., 2005, A&A, 436, 75
Humphreys E. M. L. , Greenhill L. J., Reid M. J., Beuther H., Moran J. M., Gurwell M., Wilner D. J., Kondratko P. T., 2005, ApJ, 634, L133
Humphreys E. M. L., Vlemmings W. H. T., Impellizzeri C. M. V., Galametz M., Olberg M., Conway J. E., Belitsky V., De Breuck C., 2016, A&A, 592, L13
Imanishi M., Ueno S., 1999, ApJ, 527, 709
Imanishi M., Nakanishi K., Tamura Y., Oi N., Kohno K., 2007, AJ, 134, 2366
Imanishi M., Nakagawa T., Ohyama Y., Shirahata M., Wada T., Onaka T., Oi N., 2008, PASJ, 60, S489
Imanishi M., Nakanishi K., Tamura Y., Peng C.-H., 2009, AJ, 137, 3581
Imanishi M., Nakanishi K., Izumi T., 2016, AJ, 152, 218
Imanishi M., Nakanishi K., Izumi T., 2018, ApJ, 856, 143
Imanishi M., Nakanishi K., Izumi T., 2019, ApJS, 241, 19
Imanishi M. et al., 2020, ApJ, 902, 99
Impellizzeri C. M. V., McKean J. P., Castangia P., Roy A. L., Henkel C., Brunthaler A., Wucknitz O., 2008, Nature, 456, 927
Izumi T. et al., 2016, ApJ, 818, 42
Jia J., Ptak A., Heckman T. M., Braito V., Reeves J., 2012, ApJ, 759, 41
Kewley L. J., Heisler C. A., Dopita M. A., Lumsden S., 2001, ApJS, 132, 37
Koekemoer A. M., Henkel C., Greenhill L. J., Dey A., van Breugel W., Codella C., Antonucci R., 1995, Nature, 378, 697
Kohno K., 2005, in Hüttemeister S., Manthey E., Bomans D., Weis K., eds, AIP Conf. Proc. Vol. 783, The Evolution of Starbursts. Am. Inst. Phys., New York, p. 203
Kondratko P. T., Greenhill L. J., Moran J. M., 2006a, ApJ, 652, 136
Kondratko P. T. et al., 2006b, ApJ, 638, 100
Konig S. et al., 2017, A&A, 602, 42
Krips M., Neri R., Garcia-Burillo S., Martin S., Combes F., Gracia-Carpio J., Eckart A., 2008, ApJ, 677, 262
Kuo C. Y. et al., 2011, ApJ, 727, 20
Leroy A. K. et al., 2017, ApJ, 835, 217
Maloney P. R., 2002, Publ. Astron. Soc. Aust., 19, 401
Melnick J., Mirabel I. F., 1990, A&A, 231, L19
Mirabel I. F., Lutz D., Maza J., 1991, A&A, 243, 367
Miyoshi M., Moran J., Herrnstein J., Greenhill L., Nakai N., Diamond P., Inoue M., 1995, Nature, 373, 127

Nardini E., Risaliti G., Salvati M., Sani E., Watabe Y., Marconi A., Maiolino R., 2009, MNRAS, 399, 1373
Nardini E., Risaliti G., Watabe Y., Salvati M., Sani E., 2010, MNRAS, 405, 2505
Neufeld D. A., Melnick G. J., 1991, ApJ, 368, 215
Neufeld D. A., Maloney P. R., Conger S., 1994, ApJ, 436, L127
Pappa A., Georgantopoulos I., Stewart G. C., 2000, MNRAS, 314, 589
Pesce D. W., Braatz J. A., Impellizzeri C. M. V., 2016, ApJ, 827, 68
Reunanen J., Tacconi-Garman L. E., Ivanov V. D., 2007, MNRAS, 382, 951
Risaliti G. et al., 2003, ApJ, 595, L17
Sanders D. B., Mirabel I. F., 1996, ARA&A, 34, 749
Solomon P. M., Vanden Bout P. A., 2005, ARA&A, 43, 677
Vanzi L., Bagnulo S., Le Floc'h E., Maiolino R., Pompei E., Walsh W., 2002, A&A, 386, 464
Yang C., Gao Y., Omont A., 2013, ApJ, 771, L24
Yates J. A., Field D., Gray M. D., 1997, MNRAS, 285, 303

This paper has been typeset from a TEX/LATEX file prepared by the author.